frontiers in Chemistry

ORIGINAL RESEARCH
published: 25 March 2021
doi: 10.3389/fchem.2021.647816

New Cationic *fac*-[Re(CO)$_3$(deeb)B2]$^+$ Complex, Where B2 Is a Benzimidazole Derivative, as a Potential New Luminescent Dye for Proteins Separated by SDS-PAGE

Alexander Carreño[1], Manuel Gacitúa[2], Eduardo Solis-Céspedes[3,4], Dayán Páez-Hernández[1], Wesley B. Swords[5], Gerald J. Meyer[5], Marcelo D. Preite[6], Ivonne Chávez[7], Andrés Vega[8,9] and Juan A. Fuentes[10]**

[1]Center of Applied NanoSciences (CANS), Facultad de Ciencias Exactas, Universidad Andres Bello, Santiago, Chile, [2]Facultad de Química y Biología, USACH, Santiago, Chile, [3]Escuela de Bioingeniería Médica, Facultad de Medicina, Universidad Católica del Maule, Talca, Chile, [4]Laboratorio de Bioinformática y Química Computacional, Facultad de Medicina, Universidad Católica del Maule, Talca, Chile, [5]Department of Chemistry, University of North Carolina at Chapel Hill, Chapel Hill, NC, United States, [6]Departamento de Química Orgánica, Facultad de Química y Química y de Farmacia, Pontificia Universidad Católica de Chile, Santiago, Chile, [7]Departamento de Química Inorgánica, Facultad de Química y Química y de Farmacia, Pontificia Universidad Católica de Chile, Santiago, Chile, [8]Departamento de Ciencias Químicas, Facultad de Ciencias Exactas, Universidad Andres Bello, Viña del Mar, Chile, [9]Centro para el Desarrollo de la Nanociencia y la Nanotecnología Cedenna, Santiago, Chile, [10]Laboratorio de Genética y Patogénesis Bacteriana, Facultad de Ciencias de la Vida, Universidad Andrés Bello, Santiago, Chile

OPEN ACCESS

Edited by:
Muhammad Hanif,
The University of Auckland,
New Zealand

Reviewed by:
Qianxiong Zhou,
Technical Institute of Physics and Chemistry (CAS), China
Zhe Liu,
Qufu Normal University, China

***Correspondence:**
Alexander Carreño
alexander.carreno@unab.cl
Juan A. Fuentes
jfuentes@unab.cl

Specialty section:
This article was submitted to Inorganic Chemistry, a section of the journal Frontiers in Chemistry

Received: 30 December 2020
Accepted: 29 January 2021
Published: 25 March 2021

Citation:
Carreño A, Gacitúa M, Solis-Céspedes E, Páez-Hernández D, Swords WB, Meyer GJ, Preite MD, Chávez I, Vega A and Fuentes JA (2021) New Cationic fac-[Re(CO)$_3$(deeb)B2]$^+$ Complex, Where B2 Is a Benzimidazole Derivative, as a Potential New Luminescent Dye for Proteins Separated by SDS-PAGE. Front. Chem. 9:647816. doi: 10.3389/fchem.2021.647816

Sodium-dodecyl-sulfate polyacrylamide gel electrophoresis (SDS-PAGE) can be used to separate proteins based mainly on their size such as in denaturing gels. Different staining methods have been reported to observe proteins in the gel matrix, where the most used dyes are generally anionic. Anionic dyes allow for interactions with protonated amino acids, retaining the dye in the proteins. Fluorescent staining is an alternative technique considered to be sensitive, safe, and versatile. Some anionic complexes based on d^6 transition metals have been used for this purpose, where cationic dyes have been less explored in this context. In this work, we synthesized and characterized a new monocationic rhenium complex *fac*-[Re(CO)$_3$(**deeb**)**B2**]$^+$ (where **deeb** is 4,4′-bis(ethoxycarbonyl)-2,2′-bpy and **B2** is 2,4-di-*tert-butyl*-6-(3H-imidazo[4,5-c]pyridine-2-yl)phenol). We carried out a structural characterization of this complex by MS$^+$, FTIR, ^{1}H NMR, D_2O exchange, and HHCOSY. Moreover, we carried out UV-Vis, luminescence, and cyclic voltammetry experiments to understand the effect of ligands on the complex's electronic structure. We also performed relativistic theoretical calculations using the B3LYP/TZ2P level of theory and R-TDDFT within a dielectric continuum model (COSMO) to better understand electronic transitions and optical properties. We finally assessed the potential of *fac*-[Re(CO)$_3$(**deeb**)**B2**]$^+$ (as well as the precursor *fac*-Re(CO)$_3$(**deeb**)Br and the free ligand **B2**) to stain proteins separated by SDS-PAGE. We found that only *fac*-[Re(CO)$_3$(**deeb**)**B2**]$^+$ proved viable to be directly used as a luminescent dye for proteins, presumably due to its interaction with negatively charged residues in proteins and by weak interactions provided by **B2**. In addition, *fac*-[Re(CO)$_3$(**deeb**)**B2**]$^+$ seems to interact preferentially with proteins and not with the gel matrix despite the presence of sodium dodecyl sulfate (SDS). In future

applications, these alternative cationic complexes might be used alone or in combination with more traditional anionic compounds to generate counterion dye stains to improve the process.

Keywords: rhenium(I) tricarbonyl, cyclic voltammetry, relativistic DFT, ZFS, protein dye, SDS-PAGE, protein, fluorescent stain

HIGHLIGHTS

1. Rhenium(I) complexes can be used to stain proteins
2. We synthesized and characterized a new cationic *fac*-$[Re(CO)_3(\mathbf{deeb})\mathbf{B2}]^+$ complex
3. *fac*-$[Re(CO)_3(\mathbf{deeb})\mathbf{B2}]^+$ properties are shown (UV-Vis, luminescence, and voltammetry)
4. Relativistic DFT, TD-DFT, and SOC-TDDFT calculations were performed
5. *fac*-$[Re(CO)_3(\mathbf{deeb})\mathbf{B2}]^+$ can be used as a fluorescent protein dye in SDS-PAGE

INTRODUCTION

Gel electrophoresis is a widely used molecular biology technique aimed to separate biomolecules with high resolution, which allows for multiple applications. Electrophoresis can be used to separate proteins based on their charge-to-mass ratio, shape, and size (non-denaturing gels) or based mainly on their size (denaturing gels) (Zewert and Harrington, 1993). In denaturing gels, sodium dodecyl sulfate (SDS), which coats the denatured protein through hydrophobic interactions, maintains the unfolded state due to SDS electrostatic repulsions. Consequently, negative charges provided by SDS dominate the total charge of proteins in an aqueous solution. This denaturing technique is known as sodium-dodecyl-sulfate polyacrylamide gel electrophoresis (SDS-PAGE) (Maizel, 2000; Samdin et al., 2020).

In order to observe proteins in the gel matrix, it is necessary to use staining methods. Some of these methods include colorimetric total protein stains, such as silver stain, considered one of the most sensitive procedures for detecting proteins; zinc staining, a negative method that stains the polyacrylamide gel only in regions where there are no proteins; and Coomassie brilliant blue (CBB; disulfonated triphenylmethane dye), one of the most used dyes (Rabilloud, 1990; Wirth and Romano, 1995; Patton, 2002; Sundaram et al., 2012). CBB binds to proteins via electrostatic interactions of the sulfonate ($-SO_3^-$) groups with protonated amino acids ($-NH_3^+$ or $-NH^+-$) (i.e., lysine, arginine, or histidine) but also by hydrophobic interactions with the exposed aromatic residues (i.e., phenylalanine, tyrosine, and tryptophan) (Sundaram et al., 2012).

Fluorescent staining is an alternative technique that offers some exciting features. It has been stated that fluorescent staining presents higher linear quantitation ranges than colorimetric methods (Sundaram et al., 2012). Fluorescent protein gel staining is considered a technique that is sensitive, safe, and versatile. Although detection depends on a device providing a suitable excitation wavelength, common transilluminators, ordinarily present in molecular biology laboratories, can be used for this purpose. A device with a light-emitting diode or another source of filtered light, coupled with a filter for the emission, is sufficient to observe many of the UV-excitable dyes (Sundaram et al., 2012).

Some fluorescent stainings for proteins have been described. Epicocconone stain is an azaphilone that reacts with primary amines in proteins, generating a red fluorescent compound (Bell and Karuso, 2003). Nile red (Nile blue oxazone) is a phenoxazone that presents fluorescence enhancement in the presence of protein–SDS complexes, which makes it useful for SDS-PAGE (Sundaram et al., 2012). On the other hand, metal-based fluorescent dyes have also been reported. SYPRO^{TM} Ruby (a ruthenium-based compound whose formulation is held secret for commercial purposes) presents high sensitivity to proteins, which is equivalent to the silver staining method and independent of the presence of nucleic acids and lipopolysaccharides (Sundaram et al., 2012).

In the frame of the development of new fluorescent dyes to stain proteins, d^6 transition metals can be considered, including Ru(II), Ir(III), and Re(I). d^6 transition metals show useful photophysical properties, including visible-light absorption and emission, chemical stability, and low cytotoxicity (Fernandez-Moreira et al., 2010; Thorp-Greenwood et al., 2012; Carreño et al., 2019; Otero et al., 2019; Carreño et al., 2021). In addition, d^6 transition-metal complexes have shown interesting biological applications not only as fluorophores but also in other areas such as selective cytotoxic complexes against cancer cells (Tian et al., 2017; Xu et al., 2018; Balaji et al., 2020; Li et al., 2020).

Regarding the d^6 transition-metal complexes to stain proteins, Ru(II) bathophenanthroline disulfonate (RuBPS) is a luminescent complex that efficiently stains proteins in polyacrylamide gels (Rabilloud et al., 2001; Babak et al., 2020). This feature can be attributed to the bathophenanthroline disulfonate moiety, which allows water solubility and permits electrostatic interactions similar to that described for CBB (Graham et al., 1978; Berggren et al., 2000; Steinberg et al., 2000; Rabilloud et al., 2001). The bathophenanthroline disulfonate (BPS) moiety has been used to generate alternative d^6 complexes to stain proteins in the polyacrylamide gels, including $Ir(C,N)_2(BPS)$ (Jia et al., 2012).

Regarding the use of Re(I) complexes, it has been reported that Re(I)-tetrazolato complexes *fac*-$[Re(CO)_3(N,N)(Tph)]^{0/+/2-}$, where Tph is 5-phenyl-tetrazolato, have been analyzed as luminescent dyes for proteins separated by electrophoresis

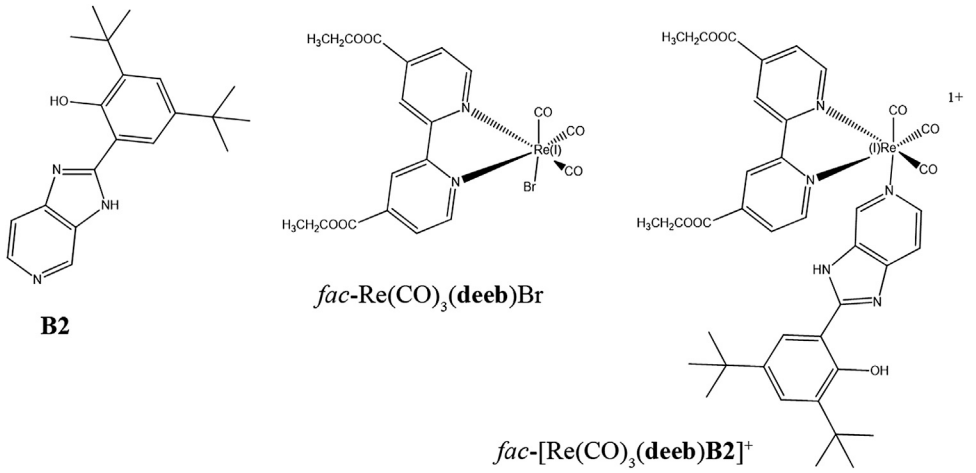

SCHEME 1 | Chemical structure of **B2** [2,4-di-*tert*-butyl-6-(3H-imidazo[4,5-c]pyridine-2-yl)phenol], *fac*-Re(CO)$_3$(**deeb**)Br, and *fac*-[Re(CO)$_3$(**deeb**)**B2**]$^+$.

(SDS-PAGE) (Fiorini et al., 2018). In that study, the authors explored different equatorial ligands, such as bathophenanthroline disulfonate (BPS) or bathocuproine disulfonate (BC), yielding *fac*-[Re(CO)$_3$(BPS)(Tph)]$^{2-}$ and *fac*-[Re(CO)$_3$(BC)(Tph)]$^{2-}$. As expected, these two anionic complexes successfully marked proteins separated by SDS-PAGE due to disulfonate groups (Fiorini et al., 2018). Although the presence of the disulfonate groups has been widely used to achieve the (dye-SO_3^-/$^+NH_3$–protein) interaction, as stated above, other strategies can also be used (Jin and Choi, 2004). Cationic dyes can also interact with proteins, presumably by electrostatic interactions with negatively charged residues (e.g., the presence of –COO^- in aspartate and glutamate) (Jin and Choi, 2004). The cationic complex *fac*-[Re(CO)$_3$(BC)(Tph-Me)]$^+$, where Tph-Me corresponds to 5-phenyl-4-methyl-tetrazolato, is also able to stain proteins but with reduced sensitivity in comparison with complexes harboring sulfonate groups. In order to improve these kinds of cationic complexes, new ancillary ligands have been reported as useful to modulate different properties. Since hydrophobic interactions, van der Waals forces, and hydrogen bonding can also contribute to the binding of the dye to proteins (Jin and Choi, 2004; Fiorini et al., 2018), the exploration of new ligands could allow obtaining alternative complexes to stain proteins, especially when considering the timesaving synthesis of sulfonated-free complexes (Fiorini et al., 2018). In this context, an ancillary ligand allowing for the formation of hydrophobic interactions, van der Waals forces, and/or hydrogen bonding with proteins could contribute to this development, even with cationic complexes.

The exploration of other luminescent molecules in biological applications has already been reported. **B2** [2,4-di-*tert*-butyl-6-(3H-imidazo[4,5-c]pyridine-2-yl)phenol] presents promising features regarding its use as a fluorophore for diverse biological applications. **B2** is an excellent luminescent cell dye for confocal microscopy, showing differential staining for the endoplasmic reticulum and the Golgi apparatus in epithelial cell lines (Carreno et al., 2016a; Llancalahuen et al., 2018) and staining walled cells, such as yeasts (*Candida albicans*), Gram-negative bacteria (*Salmonella enterica* and *Escherichia coli*), and Gram-positive bacteria (*Lactobacillus kunkeei*) for confocal microscopy (Carreno et al., 2016a; Berrios et al., 2018). Nevertheless, despite these remarkable properties, **B2** lacks sulfonate groups (–SO_3^-) and positively charged groups, suggesting that this compound cannot interact with proteins to permit an efficient protein staining. Therefore, we sought to generate a fluorescent dye for protein staining based on **B2**. In this work, we report the synthesis of a new complex *fac*-[Re(CO)$_3$(**deeb**)**B2**]$^+$ [where **deeb** is 4,4′-bis(ethoxycarbonyl)-2,2′-bipyridine], which was synthesized by replacing –Br from *fac*-Re(CO)$_3$(**deeb**)Br (Hasselmann and Meyer, 1999b; Carreno et al., 2015; Carreño et al., 2017a) with **B2** (**Scheme 1**). The new *fac*-[Re(CO)$_3$(**deeb**)**B2**]$^+$ complex was synthesized and characterized using chemical techniques such as FTIR, ^{1}H NMR, HHCOSY, mass spectrometry (EI-MS 894.3 M$^+$), UV-Vis, emission, and cyclic voltammetry. We also performed a relativistic computational characterization to corroborate the experimental assignments and better understand the absorption and emission transitions. The complex showed luminescent emission with a large Stokes shift (λ_{ex} = 366 nm, λ_{em} = 625 nm), τ of 200 ns, and φ = 0.004. Finally, we found that *fac*-[Re(CO)$_3$(**deeb**)**B2**]$^+$ can fluorescently stain proteins separated by electrophoresis, presumably due to electrostatic interactions between the complex and negatively charged residues (e.g., –COO^-) (provided by its cationic nature) but also plausibly by other kinds of interactions due to the presence of **B2** as the ancillary ligand. This work underlines that the synthesis of alternative complexes, i.e., cationic complexes lacking sulfonate groups, can also be designed to stain proteins. In future applications, these alternative cationic complexes might be used alone or in combination with more traditional anionic compounds to generate counterion dye stainings.

EXPERIMENTAL AND THEORETICAL PROCEDURES

Materials and Synthesis

All starting materials were purchased from Merck and Aldrich and used with no further purification. Acetonitrile (CH_3CN) was dried in molecular sieves and purged under argon gas for electrochemical applications (Del Valle et al., 2009). Synthesis and characterization of rhenium(I) tricarbonyl complexes are described below.

Synthesis of B2 (2,4-Di-*tert*-butyl-6-(3H-imidazo [4,5-c]pyridine-2-yl)phenol)

The compound was obtained according to a procedure previously reported (Carreno et al., 2016a).

Synthesis of *fac*-Re(CO)$_3$(deeb)Br

The complex was obtained as previously reported (Hasselmann and Meyer, 1999a). In this case, we used $(Re(CO)_3Br(THF))_2$ dimer and **deeb** as starting materials (Carreno et al., 2015).

Synthesis of *fac*-[Re(CO)$_3$(deeb)B2]$^+$

A suspension of *fac*-Re(CO)$_3$(**deeb**)**Br** (in anhydrous THF) was added to $Ag^+(O_3SCF_3)^-$ (1:1 M ratio) under an inert atmosphere in the dark. The mixture was stirred at room temperature for 2–3 h under nitrogen. The precipitated AgBr byproduct was removed by filtration, and then **B2** (dissolved in anhydrous THF) (1:1 M ratio) was added before refluxing for 5 h under nitrogen (Carreno et al., 2015). The solution was concentrated using a rotary evaporator, and the solid residue was dissolved in ethanol. Excess NH_4PF_6 was added, and the mixture was stirred for 24 h. The solid was precipitated, collected, and recrystallized from ethanol/diethyl ether (1:1, v/v). Yield = around 70.0%. FTIR (cm^{-1}): 3331 and 3125 (νOH), 2034 and 1925 (νCO), 1777 (νCO), 832 (νPF_6^-). ESI-MS Calcd (found) for $ReC_{39}H_{41}N_5O_8$: m/z $^+$ 893.96 (894.3). ^{1}H NMR (400 MHz, CD_3CN): δ = 1.35 [s, 9H], 1.42 [s, 9H], 5.59 [s, 2H, –NH_2], 6.45 [d; J = 5.5 Hz; 1H], 7.28 [d; J = 1.5 Hz; 1H], 7.43 [s, 1H], 7.51 [s, 1H], 7.53 [s, 1H], 7.77 [dd; J = 5.5; 7.9 Hz; 2H], 8.11 [s, 1H], 8.28 [dd; J = 5.6; 7.9 Hz; 2H], 8.39 [d; J = 8.3 Hz; 2H], 8.91 [s, 1H], 9.21 [d; J = 5.6 Hz; 2H], 12.54 [s, –OH]. UV-Vis (acetonitrile, room temperature): λ = 338 nm.

Physical Measurements

FTIR spectra were obtained on a Bruker Vector-22 FT-IR spectrophotometer. The ^{1}H NMR spectra for **B2**, *fac*-Re(CO)$_3$(**deeb**)**Br**, and *fac*-[Re(CO)$_3$(**deeb**)**B2**]$^+$ were recorded on a Bruker AVANCE 400 spectrometer at 400 MHz at 25°C. The sample was dissolved in deuterated solvents (DMSO-$_{d6}$ or acetonitrile-$_{d3}$) using tetramethylsilane as an internal reference. The UV-Vis absorption spectrum for *fac*-[Re(CO)$_3$(**deeb**)**B2**]$^+$ was recorded using a Varian Cary 60 UV-Vis spectrophotometer with a resolution of 1 nm. The steady-state photoluminescence spectrum for *fac*-[Re(CO)$_3$(**deeb**)**B2**]$^+$ was measured on an ISS K2 fluorometer. The samples were sparged with argon-saturated acetonitrile for 30 min and excited at λ ~445 nm. The intensity was integrated for 0.5 s with a 2 nm resolution. The photoluminescence quantum yield was measured through comparative actinometry using [Ru(2,2′-bipyridine)$_3$][PF_6]$_2$ in acetonitrile (φ_{em} = 0.06) as a quantum yield standard (Bond et al., 2002; Hess et al., 2017). Photoluminescence lifetime measurements were performed using a PTI nitrogen dye laser with excitation centered around 445 nm. Decays were monitored at the photoluminescence maximum and averaged over 180 scans.

The mass spectra of *fac*-[Re(CO)$_3$(**deeb**)**B2**]$^+$ were analyzed with UPLC Xevo G2 Q-TOF (Waters) (high resolution mass spectrometer).

For electrochemical experiments, the working solution contained 0.01 mol/L of the respective compound (i.e., **B2**, *fac*-Re(CO)$_3$(**deeb**)Br, and *fac*-[Re(CO)$_3$(**deeb**)**B2**]$^+$) with 0.1 mol/L tetrabutylammonium hexafluorophosphate ($TBAPF_6$, supporting electrolyte) in anhydrous acetonitrile (CH_3CN). Before each experiment, the working solution was purged with high purity argon, and an argon atmosphere was maintained during the whole experiment. A polycrystalline, non-annealed platinum disc (2 mm diameter) was used as the working electrode. A platinum gauze of a large geometrical area, separated from the main cell compartment by a fine sintered glass, was used as the counter electrode (Del Valle et al., 2012; Ramírez et al., 2016). All potentials quoted in this paper are referred to as Ag/AgCl electrodes in tetramethylammonium chloride to match the potential of a saturated calomel electrode (SCE) at room temperature. All electrochemical experiments were performed at room temperature on a CHI900B bipotentiostat interfaced to a PC running CHI 9.12 software that allowed for experimental control and data acquisition.

Computational Details

All the calculations were performed using the Amsterdam Density Functional (ADF) code (Te Velde et al., 2001). The scalar relativistic and spin–orbit coupling effects were incorporated using the two-component Hamiltonian with the zeroth-order regular approximation (ZORA Hamiltonian) (Lenthe et al., 1993; Anton et al., 2004). The ground and first excited triplet state geometries were optimized at the B3LYP/TZ2P level of theory (Kim and Jordan, 1994; Stephens et al., 1994; Van Lenthe and Baerends, 2003). Implicit solvation effects on the geometry optimization and optical properties were considered using a dielectric continuum model (COSMO) with acetonitrile as a solvent (Van Lenthe and Baerends, 2003; Bickelhaupt and Baerends, 2007). The molecular structure was considered without terminal methyl groups in the bipyridine moiety to avoid convergence problems due to the group rotation. This procedure has no impact on the studied luminescent phenomena.

Scalar relativistic time-dependent density functional theory (SR-TDDFT) was used to calculate the absorption spectra for the 30 singlet and 30 triplet excitations, which were subsequently used as the basis for the self-consistent two-component spin–orbit coupling TDDFT (SOC-TDDFT) within the ZORA Hamiltonian (Wang and Ziegler, 2005; Krause and Klopper, 2015).

Protein Visualization

Bacterial strains. We worked with *Salmonella enterica* subspecies *enterica* serovar Typhimurium ATCC 14028s (simply called Typhimurium).

Bacterial culture. Bacteria were cultured under standard laboratory conditions (i.e., shaking at 37°C) in Luria–Bertani broth (Bacto tryptone, 10 g/L; NaCl, 5.0 g/L; yeast extract, 5 g/L) (Nevermann et al., 2019). Bacteria were harvested at the stationary phase (OD_{600} = 1.4).

Protein obtention. Bacteria were centrifuged for 10 min at 5400 ×*g* (4°C). The supernatant was discarded, and the pellet was washed three times with buffer Tris-HCl 10 mM pH 8.0 (Nevermann et al., 2019). Bacteria were finally resuspended in Tris-HCl 10 mM pH 8.0, 1 mM phenylmethylsulfonyl fluoride (PMSF), and 1 mM ethylenediaminetetraacetic acid (EDTA) before being sonicated on ice for 100 s. Proteins were stored at −80°C until use.

Determination of protein concentration. The total protein concentration was determined by the BCA™ Protein Assay Kit (Thermo Scientific) according to the manufacturer's instructions.

SDS-PAGE. Polyacrylamide gels (12.5%) (Nevermann et al., 2019) were prepared in BioRad™ chambers (separation gel: 2.415 µl [acrylamide 30%:bisacrylamide 0.8%], 1.320 µl buffer Tris-HCl 1.5 M pH 8.8, 52.5 µl sodium dodecyl sulfate [SDS] 10%, 955 µl distilled water, 150 µl ammonium persulfate [PSA], and 7.5 µl N,N,N′,N′-tetramethyl-ethylenediamine [TEMED]; stacking gel: 312 µl [acrylamide 30%:bisacrylamide 0.8%], 450 µl buffer Tris-HCl 0.5 M pH 6.8, 1.040 µl distilled water, 50 µl PSA, and 3.75 µl TEMED). The electrophoresis chamber was filled with running buffer (1.44% glycine, 0.3% Tris, and 0.1% SDS). Then, proteins were mixed with one volume of load buffer (187.5 mM Tris-HCl pH 6.8, 6% SDS, 30% glycerol, 0.03% bromophenol blue, and 15% β-mercaptoethanol), before being incubated at 98°C for 5 min. A total of 100 µg proteins were loaded in the respective lanes. Electrophoresis was performed at a constant voltage of 50 V until the sample reached the separation gel, where the voltage was increased to 100 V.

Protein staining. The gel was incubated for 30 min at room temperature with distilled water prior to incubating it in a solution of **B2**, *fac*-Re(CO)$_3$(**deeb**)Br, or *fac*-[Re(CO)$_3$(**deeb**)**B2**]$^+$ (400 µg/ml in DMSO) for 60 min at room temperature covered with an aluminum foil. Finally, the gel was washed with either distilled water for 10 min or DMSO 25% in distilled water for 12 h under gentle shaking. Stained proteins were observed in a UV transilluminator ECX-20M (λ_{exc} = 312 nm).

RESULTS AND DISCUSSION

Characterization of *fac*-[Re(CO)$_3$(deeb)B2]$^+$

As stated above, the *fac*-Re(CO)$_3$ (**deeb**)**Br** complex was obtained as previously reported (Hasselmann and Meyer, 1999a; Hasselmann and Meyer, 1999b). Nevertheless, in this work, *fac*-Re(CO)$_3$(**deeb**)**Br** was synthesized by an alternative method based on the reaction of the **deeb** ligand with the (Re(CO)$_3$Br(THF))$_2$ dimer (Carreno et al., 2015). On the other hand, **B2** was synthesized as reported (Carreno et al., 2016a). The ^{1}H NMR of both *fac*-Re(CO)$_3$(**deeb**)**Br** and **B2** showed expected values (**Supplementary Figures S1, 2** in the **Supplementary Material**). In order to synthesize *fac*-[Re(CO)$_3$(**deeb**)**B2**]$^+$, we used a previously reported procedure (Carreno et al., 2015), obtaining high yield (around 70%). Characteristic constants of *fac*-[Re(CO)$_3$(**deeb**)**B2**]$^+$ (i.e., molecular weight, yield, and solid color) are shown in **Supplementary Table S1** in the **Supplementary Material**. The mass spectrometric analysis (FOB) of *fac*-[Re(CO)$_3$(**deeb**)**B2**]$^+$ ($ReC_{39}H_{41}N_5O_8^{1+}$) showed a central fragment at m/z = 894.3, in agreement with the expected value for the molecular ion (it aligns with the Re^+ complex without PF_6^-). The isotope structure is consistent with the rhenium composition (**Supplementary Figure S3** in the **Supplementary Material**). The FTIR spectrum, along with both 1D and 2D ^{1}H NMR assays (see below), was used to confirm the *fac*-[Re(CO)$_3$(**deeb**)**B2**]$^+$ structure. In the FTIR spectrum, the range around 3500–3000 cm^{-1} presented bands that are generally considered symmetric and asymmetric, due to νOH and/or νNH vibrations at 3331 cm^{-1} in the **B2** moiety (**Supplementary Figure S4** in the **Supplementary Material**). We assigned the bands at 3125 cm^{-1} (aromatic νCH) and 2963 cm^{-1} and 2873 cm^{-1} (νCH). On the other hand, regarding the presence of carbonyl groups in the *fac*-[Re(CO)$_3$(**deeb**)**B2**]$^+$ complex, only two bands were observed at 2034 cm^{-1} and 1925 cm^{-1} in the FTIR spectrum. This result can be explained by a convolution of facial carbonyls due to a local symmetry loss. Thus, the carbonyl stretching was affected by the dπ electron density due to the ancillary ligand (**B2**). On the other hand, the π–back bonding effect in the carbonyls (–CO) also was observed. This effect can be explained by delocalization of electron density from the rhenium(I) metal to the carbonyl π^*-orbitals, resulting in a lowered CO stretching frequency, compared to free CO (2143 cm^{-1}) (Bistoni et al., 2016). The 1733 cm^{-1} mode was assigned to the carbonyl group of the ester groups in the **deeb** ligand. Other important modes appeared at 1617 cm^{-1}, and 1578 cm^{-1} (νCN) and 1430 cm^{-1} (νCC) in the aromatic rings, and a signal at 832 cm^{-1} was assigned to the PF_6^- anion.

The *fac*-[Re(CO)$_3$(**deeb**)**B2**]$^+$ complex was also characterized by its ^{1}H NMR spectra (1D and 2D) in acetonitrile-$_{d3}$ (for proton numbering, see **Supplementary Scheme S1**; for ^{1}H NMR, see **Supplementary Figure S5**; for the expanded aromatic region, see **Supplementary Figure S6** in the **Supplementary Material**). The **deeb** protons in the *fac*-[Re(CO)$_3$(**deeb**)**B2**]$^+$ complex were assigned at 9.40 ppm (H1′, d, J = 5.7 Hz), 9.13 ppm (H1", d, J = 5.7 Hz), 8.18 ppm (H2′, dd, J = 5.7 and 1.2 Hz), 8.09 ppm (H2", dd, J = 5.6 and 1.4 Hz), 8.93 ppm (H3′, s), and 8.79 ppm (H3", s). These results indicate that the protons of the **deeb** moiety are diastereotopic, in contrast with what was observed with the **deeb** ligand in the *fac*-Re(CO)$_3$(**deeb**)Br complex (**Supplementary Figure S1** in the **Supplementary Material**), in which the protons have the same chemical shift (homotopic). In the case of the **B2** moiety in the *fac*-[Re(CO)$_3$(**deeb**)**B2**]$^+$ complex, we observed a general displacement to higher fields in comparison with free **B2** (compare **Supplementary Figure S2** with **Supplementary Figure S5** in the **Supplementary Material**). The assignment was as follows: 8.54 ppm (H3), 7.97 ppm

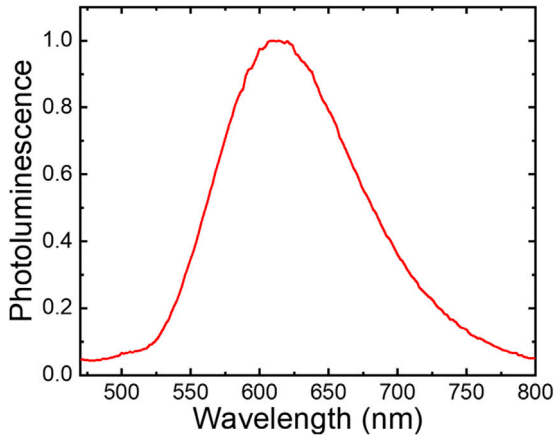

FIGURE 1 | Photoluminescence spectra of *fac*-[Re(CO)$_3$(**deeb**)**B2**]$^+$ in acetonitrile (λ_{exc} = 445 nm).

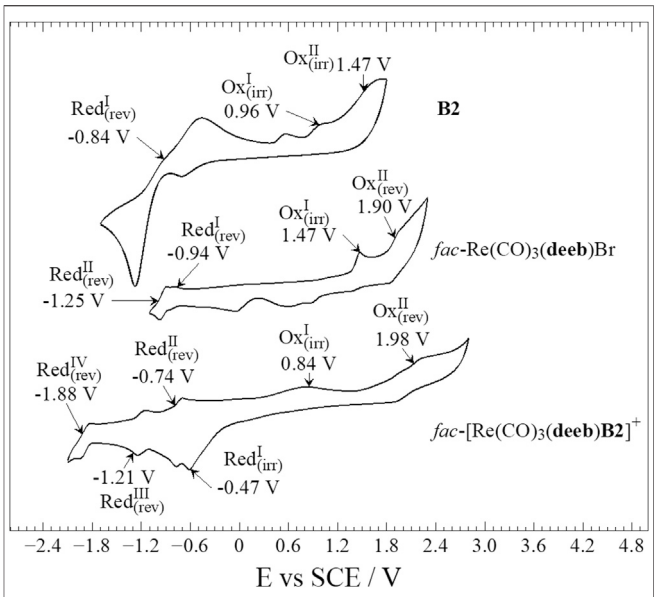

FIGURE 2 | Compared electrochemical response of **B2**, *fac*-Re(CO)$_3$(**deeb**)Br, and *fac*-[Re(CO)$_3$(**deeb**)**B2**]$^+$. Interphase: Pt|1.0 × 10^{-2} M of compound + 1.0 × 10^{-1} M TBAPF$_6$ in anhydrous CH_3CN.

TABLE 1 | Photophysical properties of the uncoordinated **B2** (Carreno et al., 2016a) ligand and *fac*-[Re(CO)$_3$(**deeb**)**B2**]$^+$.

Compound	τ (ns)	Quantum yield	k_r (M^{-1} s^{-1})	k_{nr} (M^{-1} s^{-1})
B2	<10[a]	0.21	2.1 × 10^{7b}	7.9 × 10^{7b}
fac-[Re(CO)$_3$(**deeb**)**B2**]$^+$	200	0.004	2.0 × 10^4	4.98 × 10^6

[a]*Lifetime was faster than the instrument response.*
[b]*These values are approximated.*

(H1), 7.36 ppm (H2), 7.55 ppm (H4), and 7.45 ppm (H5). The –OH and –NH groups were observed at 12.75 ppm and 5.96 ppm, respectively. These signals disappeared with D_2O exchange, confirming the assignation (**Supplementary Figure S7** in the **Supplementary Material**).

On the other hand, the resonances of aromatic protons found in the **deeb** ligand in *fac*-[Re(CO)$_3$(**deeb**)**B2**]$^+$ showed lower values compared to those of the corresponding *fac*-Re(CO)$_3$(**deeb**)Br precursor, suggesting that **B2** may be a weaker electron-donating group compared with –Br or may exert a withdrawing effect over the Re(I) core (compare **Supplementary Figures S1 and 5** in the **Supplementary Material**).

Other signals were assigned at 1.25 ppm and 1.35 ppm corresponding to the *tert*-butyl protons in **B2** and at 4.39 ppm (q, –CH_2–) and 1.40 ppm (t, –CH_3–) corresponding to the **deeb** moiety (**Supplementary Figure S5** in the **Supplementary Material**). The HHCOSY experiment confirmed the assignments (**Supplementary Figure S8** in the **Supplementary Material**). The FTIR, MS$^+$, and ^{1}H NMR assays, together, confirmed the proposed structure.

The absorption spectrum of *fac*-[Re(CO)$_3$(**deeb**)**B2**]$^+$ in acetonitrile was recorded at room temperature. The *fac*-[Re(CO)$_3$(**deeb**)**B2**]$^+$ complex showed the expected absorption bands for this kind of compound (Carreno et al., 2015; Carreno et al., 2016b; Carreño et al., 2017b) centered around 284 nm and 335 nm. In addition, we observed a third, not very intense, band centered around 405 nm (**Supplementary Figure S9** in the **Supplementary Material**). The composition of these bands is discussed below. This spectrum was blue-shifted relative to the *fac*-Re(CO)$_3$(**deeb**)Br precursor, which showed intense adsorption bands centered at 312 nm and 419 nm, as reported previously (Hasselmann and Meyer, 1999a; Hasselmann and Meyer, 1999b). This blue shifting may be attributed to the π-acidic nature of **B2** compared with Br present in *fac*-Re(CO)$_3$(**deeb**)Br, although the difference in electronic effect between **B2** and –**Br** may play a more significant role. The blue shifting has already been reported for similar compounds with ancillary ligands presenting intramolecular hydrogen bonds (Carreno et al., 2015; Carreno et al., 2016b; Carreño et al., 2017b).

Steady-state 445 nm light excitation of *fac*-[Re(CO)$_3$(**deeb**)**B2**]$^+$ in acetonitrile resulted in room temperature photoluminescence with a broad band centered around λ_{max} = 615 nm (**Figure 1**). Thus, a large Stokes-like shift was observed, consistent with a large change in the dipole moment between the ground and excited states (emission lifetime = 200 ns, φ = 0.004). These emission processes are characteristic of rhenium(I) tricarbonyl complexes and agree with the long-lived ^{3}MLCT excited states (Thorp-Greenwood et al., 2016; Malecka et al., 2020; Maron et al., 2020; Carreño et al., 2021).

Table 1 summarizes the photophysical properties of **B2** and the new complex *fac*-[Re(CO)$_3$(**deeb**)**B2**]$^+$. We attribute the low quantum yield of *fac*-[Re(CO)$_3$(**deeb**)**B2**]$^+$, compared with its precursor *fac*-Re(CO)$_3$(**deeb**)Br in the excited states (quantum yield = 0.030, τ = 30 ns (Hasselmann and Meyer, 1999a)), to intramolecular electron transfer in the ^{3}MLCT excited state initiated by the presence of a redox-active phenol group (see below) coupled to proton transfer from phenol to nitrogen in the **B2** moiety. Such intramolecular quenching has been previously

reported through flash quench experiments of a ruthenium bipyridine complex (Zhang et al., 2011; Nomrowski and Wenger, 2015; Lennox et al., 2017). The proton-coupled electron transfer has also been observed for rhenium(I) tricarbonyl complexes in intermolecular interactions (Manbeck et al., 2016; Prado et al., 2016; Pannwitz and Wenger, 2019). The presence of the intramolecular hydrogen bond (IHB) in **B2** could also be contributing to the relatively low quantum yield in the *fac*-[Re(CO)$_3$(**deeb**)**B2**]$^+$ complex. It has been reported for similar Re(I) complexes harboring ancillary ligands with an IHB that the quantum yields can be improved by disrupting the IHB with a mixture of D_2O/CH_3CN (Carreno et al., 2016b). Thus, it would be possible to achieve similar effects by synthesizing a **B2** derivative lacking −OH involved in the IHB. Nevertheless, this hypothesis remains to be experimentally tested.

Electrochemical Behavior

In order to further characterize *fac*-[Re(CO)$_3$(**deeb**)**B2**]$^+$, we compared its electrochemical behavior with that of its precursor *fac*-Re(CO)$_3$(**deeb**)Br (Carreno et al., 2015) and its ancillary ligand **B2** (Carreno et al., 2016a). Our analysis is shown in **Figure 2**.

Regarding the electrochemical response of *fac*-Re(CO)$_3$(**deeb**)Br, we found irreversible oxidation of rhenium at E_p + 1.47 V, according to the previously reported value (Hasselmann and Meyer, 1999a; Carreno et al., 2015). In the present study, we found a second reversible oxidation at $E_{½}$ + 1.90 V (**Figure 2**). This process was observed due to an increase in the potential limit explored. These oxidation processes follow an electrochemical–chemical–electrochemical reaction (ECE) mechanism (Czerwieniec et al., 2005; Canales et al., 2017; Lindley et al., 2018) with the following steps: 1) first electrochemical one-electron oxidation of the rhenium center, $Re^{I\rightarrow II}$, followed by 2) an intramolecular Re/ligand redox process, $Re^{II\rightarrow I}$, with the ligand (Br) substitution by solvent molecules, and ending with 3) a second electrochemical one-electron oxidation of the rhenium center, $Re^{I\rightarrow II}$.

In the case of *fac*-[Re(CO)$_3$(**deeb**)**B2**]$^+$, two oxidations were found (see the working window study in **Supplementary Figures S10 and 11** and in the **Supplementary Material**). The first oxidation was determined to be irreversible at E_p + 0.84 V and possibly corresponds to one of the irreversible processes in the **B2** moiety; the other oxidation process in the **B2** moiety may not take place or be masked due to the intense oxidation current from the second oxidation in *fac*-[Re(CO)$_3$(**deeb**)**B2**]$^+$. This second oxidation was reversible at $E_{½}$ + 1.98 V and most likely corresponds to the $Re^{I\rightarrow II}$ process (**Figure 2**). Thereby, the presence of the **B2** ligand in *fac*-[Re(CO)$_3$(**deeb**)**B2**]$^+$, compared with *fac*-Re(CO)$_3$(**deeb**)Br, produces a strong potential shift for the first step on the ECE mechanism 1) $Re^{I\rightarrow II}$ to a higher energy value. This result agrees with the proposed electron-withdrawing nature of the **B2** moiety in *fac*-[Re(CO)$_3$(**deeb**)**B2**]$^+$ (see the NMR and absorption study), which decreases the possibility (i.e., it increases the required potential) to accomplish the rhenium center oxidation.

TABLE 2 | Electrochemical characterization summary of *fac*-[Re(CO)$_3$(deeb)B2]$^+$.

	Potential (V)	Reversibility	Diffusion control?	Designation
Ox^I	Ep +0.84	Irreversible	Yes	**B2** oxidation
Ox^{II}	$E_{½}$ +1.98	Reversible	Yes	$Re^{I\rightarrow II}$, with **B2** elimination
Red^I	Ep −0.47	Irreversible	Yes	**B2** reduction
Red^{II}	$E_{½}$ −0.74	Reversible	Yes	**deeb** reduction
Red^{III}	$E_{½}$ −1.21	Reversible	Yes	$Re^{I\rightarrow 0}$
Red^{IV}	$E_{½}$ −1.88	Reversible	Yes	$Re^{I\rightarrow 0}$, with $\mathbf{B2}^-$ elimination

Concerning the reduction processes observed, it has been reported that the free **deeb** ligand presents a reversible reduction process at $E_{½}$ −0.90 V, whereas free **B2** exhibits a strong quasi-reversible reduction process at $E_{½}$, −0.84 V vs. SCE (Carreno et al., 2015; Carreno et al., 2016a). It is worth mentioning that the reported analyses were carried out under the same experimental condition used in this study (**Figure 2**). As previously reported, the **deeb** ligand reduction shifts from −0.90 V to −0.94 V in *fac*-Re(CO)$_3$(**deeb**)**Br**, with reversible rhenium reduction $Re^{I\rightarrow 0}$ appearing at $E_{½}$ −1.25 V (Wallace and Rillema, 1993; Lo et al., 2004; Zeng et al., 2012; Carreno et al., 2015). In the case of *fac*-[Re(CO)$_3$(**deeb**)**B2**]$^+$, we found four reduction processes determined after the working window potential study (**Supplementary Figures S10, 11**). The first reduction process at Ep −0.47 V can be attributed to the **B2** moiety since this is the more intense and irreversible process. On the other hand, the reversible reduction at $E_{½}$ −0.74 V found for *fac*-[Re(CO)$_3$(**deeb**)**B2**]$^+$ was attributed to the **deeb** ligand due to its similarity to that previously reported in potential terms (around $E_{½}$ −0.90 V) (Carreno et al., 2015).

Finally, both reversible reductions at $E_{½}$ −1.21 and −1.88 V correspond to $Re^{I\rightarrow 0}$ but following different alternate pathways. At $E_{½}$ −1.21 V, the rhenium reduction takes place, followed by intramolecular reduction and elimination of **B2** in its reduced form, $\mathbf{B2}^-$:

$$fac-[Re^{I}(CO)_3(\boldsymbol{deeb})\boldsymbol{B2}]^+ + e^- \rightleftharpoons fac-[Re^{0}(CO)_3(\boldsymbol{deeb})\boldsymbol{B2}]^0 \quad E_{1/2}: -1.21\ V\ (i),$$
$$fac-[Re^{0}(CO)_3(\boldsymbol{deeb})\boldsymbol{B2}]^0 \rightarrow fac-[Re^{I}(CO)_3(\boldsymbol{deeb})]^+ + \boldsymbol{B2}^-\ \ slow\ (ii).$$

Since (ii) is slow, the *fac*-[Re(CO)$_3$(deeb)B2]$^-$ species may suffer a second reduction process at a more negative potential. Thus, a second reduction takes place at $E_{½}$ −1.88 V:

$$fac-[Re^{0}(CO)_3(\boldsymbol{deeb})\boldsymbol{B2}]^0 + e^- \rightleftharpoons fac-[Re^{0}(CO)_3(\boldsymbol{deeb})\boldsymbol{B2}]^- \quad E_{1/2}: -1.88\ V\ (iii),$$
$$fac-[Re^{0}(CO)_3(\boldsymbol{deeb})\boldsymbol{B2}]^- \rightarrow fac-[Re^{I}(CO)_3(\boldsymbol{deeb})]^0 + \boldsymbol{B2}^-\ \ fast\ (iv).$$

These processes correspond to a typical electrochemical–electrochemical–chemical (EEC) mechanism, previously reported for similar rhenium complexes, with **B2** elimination as the chemical step (Manbeck et al., 2015; Abdellah et al., 2017). Thus, for *fac*-[Re(CO)$_3$(**deeb**)**B2**]$^+$, $Re^{I\rightarrow 0}$ takes place at −1.21 V, while the same process occurs at −1.25 V in the *fac*-[Re(CO)$_3$(**deeb**)]Br precursor. Therefore, this result supports the electron-withdrawing nature of **B2** on the metallic core. When **B2** is present in the *fac*-[Re(CO)$_3$(**deeb**)**B2**]$^+$ complex, the reduction

TABLE 3 | Calculated absorption bands considering the solvent effect (acetonitrile).

Molecule	λ (nm)	f	Origin	Assignment
fac-[Re(CO)$_3$(**deeb**)**B2**]$^+$	311	0.111	H − 1 → L + 3 (60%); H–3 → L + 2 (40%)	π → π*
	331	0.263	H − 2 → L + 2 (75%); H–5 → L + 2 (20%)	MLCT
	335	0.631	H → L + 3 (100%)	MLCT
	346	0.458	H − 5 → L (80%); H − 2 → L + 2 (20%)	π → π* MLCT
	375	0.203	H − 2 → L + 1 (90%)	MLCT
	415	0.130	H → L + 1	MLCT

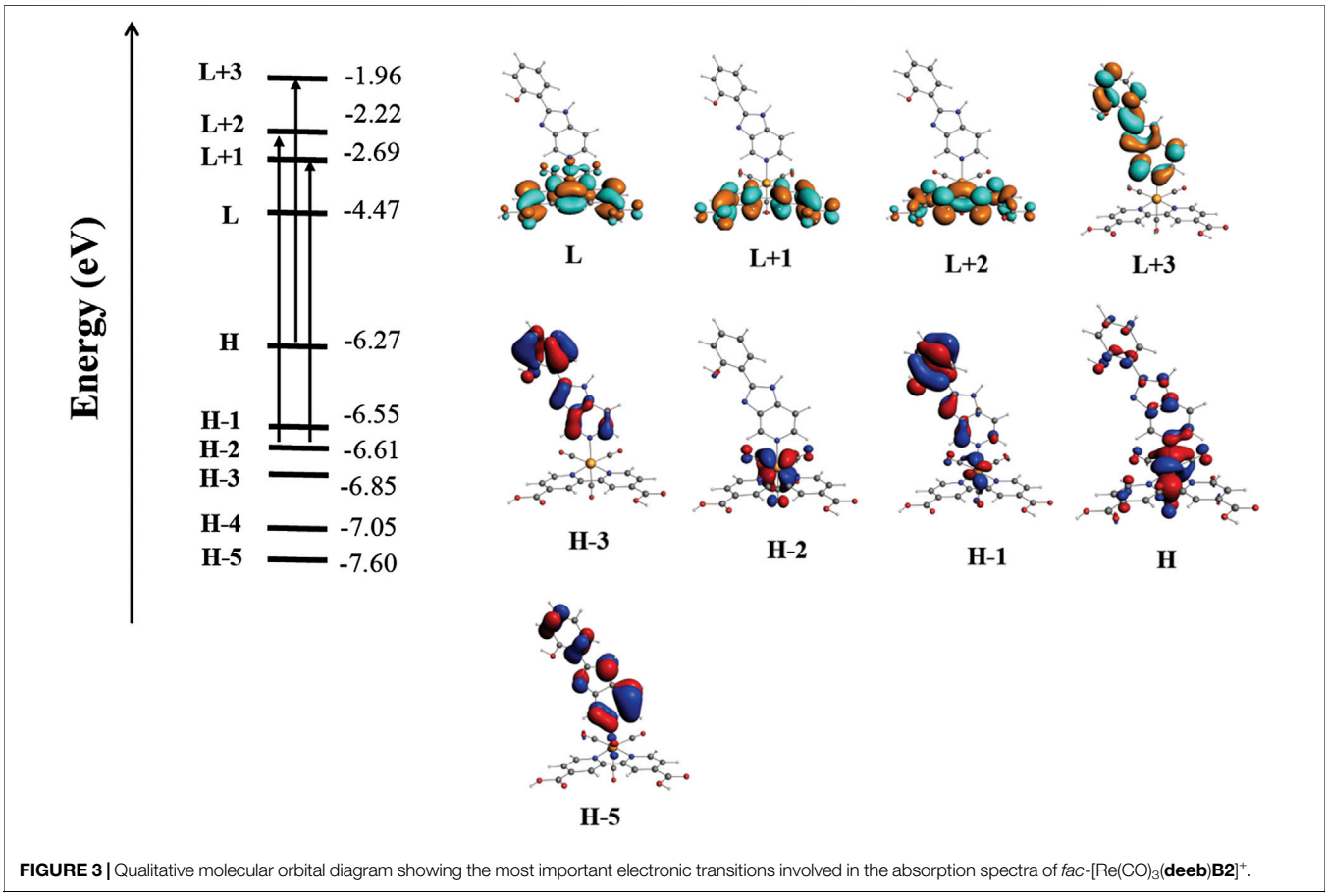

FIGURE 3 | Qualitative molecular orbital diagram showing the most important electronic transitions involved in the absorption spectra of *fac*-[Re(CO)$_3$(**deeb**)**B2**]$^+$.

shifts to less negative potential values (i.e., the reduction requires less energy to take place).

Finally, **Table 2** presents an electrochemical characterization summary for *fac*-[Re(CO)$_3$(**deeb**)**B2**]$^+$, including the electrochemical processes found, reversibility, whether they are controlled by mass transport or not (determined by a scan-rate study presented, see **Supplementary Figure S11** and **Supplementary Table S2** in the **Supplementary Material**), and the corresponding designation.

Quantum Chemistry

Although we were unable to obtain the crystal of *fac*-[Re(CO)$_3$(**deeb**)**B2**]$^+$, the computational studies were based on X-ray data obtained from a similar complex previously reported, i.e., [*fac*-Re(CO)$_3$(4,4′-dimethyl-2,2′-bpy)(*E*-2-((3-amino-pyridin-4-ylimino)-methyl)-4,6-di-*tert*-butylphenol)$^+$] (Carreño et al., 2017b).

The most important optimized bond distances and angles of *fac*-[Re(CO)$_3$(deeb)B2]$^+$ are summarized in **Supplementary Tables S3, 4, and 5** in the **Supplementary Material**. For atom numbering, see **Supplementary Figure S13** in the **Supplementary Material**. As inferred by our results, the three carbonyls of *fac*-[Re(CO)$_3$(**deeb**)**B2**]$^+$ are distributed with facial coordination according to the observed FTIR spectra (**Supplementary Figure S4** in the **Supplementary Material**). The coordination is completed by the deeb ligand in the equatorial plane and the B2 ligand in the axial plane.

Time-dependent density functional theory (R-TDDFT) (Macleod-Carey et al., 2018) calculations were performed to

TABLE 4 | Calculated emission band considering solvent effects (acetonitrile).

Molecule	Calculated λ_{em} (nm)	ZFS	f	τ (s)
fac-[Re(CO)$_3$(**deeb**)**B2**]$^+$	665	59.5	0.96×10^{-3}	2×10^{-3}

complement our analysis to elucidate and assign the calculated electronic transitions (Carreno et al., 2017; Rojas-Poblete et al., 2018). The calculated UV-Vis spectra in acetonitrile showed two principal absorption bands centered in the range 330–340 nm and 375 nm, in agreement with the experimental data. These bands were assigned as a combination of $\pi \rightarrow \pi^*$ and MLCT electronic transitions (**Table 3**, **Supplementary Figure S14** in the **Supplementary Material**). The isosurfaces of the involved molecular orbitals are shown in **Figure 3**. In this analysis, we can observe that the molecular orbitals of both the **deeb** and ancillary ligands are involved in the electronic transition. As described above, we experimentally obtained two typical bands around 284 and 335 nm. The band obtained at 284 nm corresponds to the predicted band at 311 nm, where H-1 → L + 3 corresponds to pπ(**B2**) to pπ^*(**B2**) (intraligand transition) and H-3 → L + 2 corresponds to pπ(**B2**) to pπ^*(**deeb**) (interligand transition). The band obtained experimentally around 335 nm presents a mixed composition according to our calculations. In the computed spectra, we obtained three bands with the higher harmonic oscillator (f) found in the range of 335–375 nm, which correspond to the experimental band of 335 nm. The predicted band at 335 nm is composed of H → L + 3 (100%) corresponding to [dπ(Re) and pπ(**B2**)] to pπ^*(**B2**). The calculated band at 346 nm is composed of H-5 → L (80%) and H-2 → L + 2 (20%) corresponding to dπ(**B2**) to pπ^*(**deeb**) (interligand transition) and dπ(Re) to pπ^*(**deeb**) (MLCT), respectively. The calculated band at 375 nm is composed of H-2 → L + 1 (90%) corresponding to dπ(Re) to pπ^*(**deeb**) (MLCT). The less intense band experimentally observed around 405 nm corresponds to the calculated band at 415 nm, which presents a low harmonic oscillator (**Table 3**).

Finally, the unoccupied molecular orbitals immediately around the LUMO are centered in both **deeb** and **B2**, suggesting that the ligands are directly involved in the observed emission.

To better understand the emission nature of *fac*-[Re(CO)$_3$(**deeb**)**B2**]$^+$, we carried out calculations at the SOC-TDDFT level of theory considering the solvent (acetonitrile) effect. This calculation also analyzes the three substrates derived from the excited triplet state due to spin–orbit coupling, estimating the zero-field splitting (ZFS) parameter and emission time. The calculated emission band was localized at 665 nm (**Table 4**) and assigned as ^{3}LMCT involving a π^* orbital located on **deeb** and the non-bonding, metal-centered d-orbitals. The calculated ZFS also corroborates this assignment and evidences the critical role of the metal-centered orbitals and spin–orbit coupling in the luminescent properties of *fac*-[Re(CO)$_3$(**deeb**)**B2**]$^+$. This behavior is consistent with that reported in previous studies using similar substituted bipyridines as ligands (Nastasi et al., 2015; Kia and Safari, 2016; Hostachy et al., 2017; Kang et al., 2017) and confirms that the emission occurs in the visible spectrum region.

Luminescent Staining of Proteins

As previously described, rhenium(I) tricarbonyl complexes harboring disulfonated phenanthroline-derivative ligands have been reported as useful to stain proteins separated by SDS-PAGE. Nevertheless, the use of rhenium(I) complexes lacking these ligands has been less studied to this end (Fiorini et al., 2018). In this sense, we explored whether the cationic complex *fac*-[Re(CO)$_3$(**deeb**)**B2**]$^+$, its respective precursor *fac*-Re(CO)$_3$(**deeb**)Br, or the free ligand **B2** was able to stain proteins resolved by SDS-PAGE. To that aim, a total extract of bacterial proteins was obtained before resolving them in SDS-PAGE, as indicated in *Protein Visualization in Methods*. Gels were washed with distilled water and then incubated with a solution of *fac*-[Re(CO)$_3$(**deeb**)**B2**]$^+$, *fac*-Re(CO)$_3$(**deeb**)Br, or **B2** (400 μg/ml in DMSO as solvent) for 60 min at room temperature covered with an aluminum foil. Gels were washed with either distilled water (10 min) or DMSO (25% in distilled water, 12 h) and then examined with a UV transilluminator ECX-20M (λ = 312 nm).

As shown in **Figure 4**, we observed that *fac*-[Re(CO)$_3$(**deeb**)**B2**]$^+$ could reveal the presence of proteins, as denoted by the luminescent horizontal bands in the respective lane. We did not appreciate a considerable difference by using water (10 min) or DMSO 25% (12 h) to wash the gel, in this case. This result showed that the *fac*-Re(CO)$_3$(**deeb**)**B2**]$^+$ complex interacts preferentially with proteins instead of the matrix gel. This is a very remarkable point since the matrix gel contains SDS (sodium dodecyl sulfate). The SDS, present in the gel, could interfere with a cationic dye due to its anionic nature, as previously reported (Sundaram et al., 2012). Concerning the free ligand **B2**, which is also luminescent by itself (Carreno et al., 2016a; Berrios et al., 2018; Llancalahuen et al., 2018), we observed an apparent interaction with the gel's whole matrix, showing intense luminescence even after the wash with water. When DMSO, instead of water, was used to remove unbound **B2**, we could observe some bands of high molecular weight (top of the lane), which generally retain a high amount of dye, in comparison with bands found at the bottom of the lane (low molecular weight). In this case, **B2** was not useful to stain proteins since it does not discriminate appropriately between proteins and the gel. On the other hand, when we tested the rhenium(I) precursor, i.e., *fac*-Re(CO)$_3$(**deeb**)Br, we barely could distinguish the bands corresponding to the proteins (**Figure 4**). All these results together show that the precursor alone virtually is unable to interact with proteins and remain retained, whereas the result obtained with the free ligand **B2** suggests that this compound cannot suitably distinguish between proteins and the gel. Nevertheless, the cationic complex *fac*-[Re(CO)$_3$(**deeb**)**B2**]$^+$, which is a combination of the precursor and **B2**, showed promising results, allowing for the observation of proteins under the same work conditions.

We speculate that the positive charge of *fac*-[Re(CO)$_3$(**deeb**)**B2**]$^+$ is contributing to staining proteins. Most protein dyes present an anionic nature, which allows for electrostatic

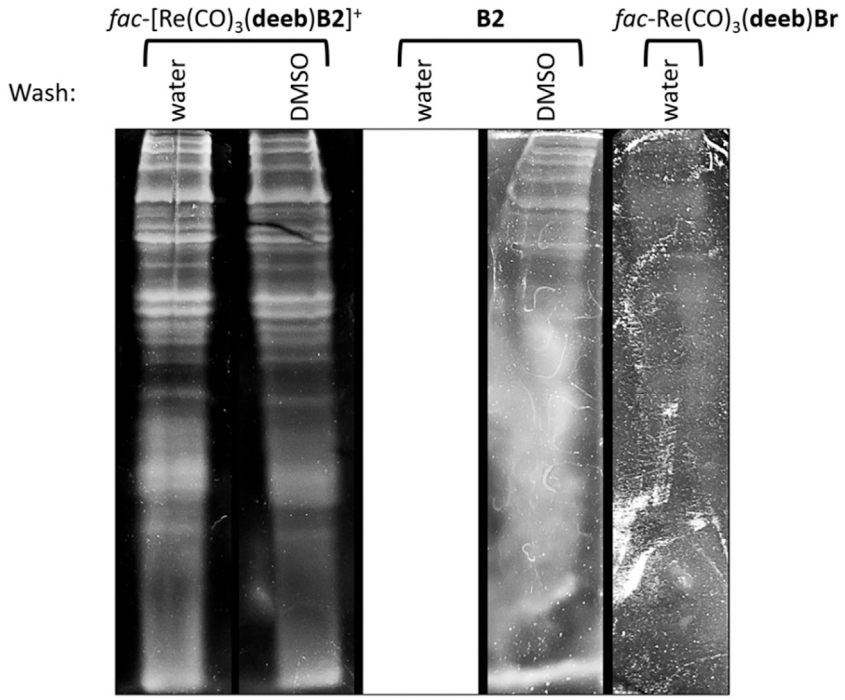

FIGURE 4 | Total proteins were extracted and resolved in SDS-PAGE before being stained with *fac*-[Re(CO)$_3$(**deeb**)**B2**]$^+$, **B2**, or *fac*-Re(CO)$_3$(**deeb**)Br for 60 min at room temperature. Gels were then washed with either distilled water (10 min) or DMSO 25% (12 h). Stained proteins were observed in a UV transilluminator ECX-20M (λ = 312 nm).

interactions with protonated amino acids (–NH_3^+ or –NH^+–) (i.e., lysine, arginine, or histidine) (Sundaram et al., 2012). Nevertheless, cationic dyes have also been reported as useful to stain proteins, which can be explained by electrostatic interactions with negatively charged residues (e.g., the presence of –COO^- in aspartate and glutamate) (Jin and Choi, 2004; Fiorini et al., 2018). We infer that the presence of the **B2** moiety in *fac*-[Re(CO)$_3$(**deeb**)**B2**]$^+$ could also be contributing to the staining capacity of this complex. It has been reported that hydrophobic interactions, van der Waals forces, and hydrogen bonding can also contribute to the binding of the dye to proteins (Jin and Choi, 2004; Fiorini et al., 2018). In this context, the **B2** moiety could participate in the interaction with proteins due to its capacity to form hydrogen bonds (Carreno et al., 2016a) and perform hydrophobic interactions (e.g., the presence of *tert*-butyls in the benzimidazole ring). In all cases, the *fac*-[Re(CO)$_3$(**deeb**)**B2**]$^+$ complex forms sufficiently strong interactions with proteins to allow staining that cannot be easily disrupted with either water or even DMSO (the solvent used to dissolve the complex). Another remarkable aspect is the selectivity regarding the interaction preferentially with the proteins and not with the gel matrix, allowing for clear visualization of bands despite the presence of SDS.

In this work, we observed that the *fac*-[Re(CO)$_3$(**deeb**)**B2**]$^+$ complex could reveal proteins separated in SDS-PAGE with a relatively simple protocol that runs for only 1 h 40 min (including gel washing, staining incubation, and destaining with water), which is a considerable shorter protocol in comparison with other classical techniques, such as CBB or silver stain (3–5 h or even more) (Fiorini et al., 2018). In the case of rhenium(I)-based staining of proteins, including cationic complexes, the reported protocol runs for approximately 14 h (Fiorini et al., 2018), underlining the potential of *fac*-[Re(CO)$_3$(**deeb**)**B2**]$^+$ as a possible precursor for the development of improved fluorescent stainings, for instance, in combination with another anionic complex to generate a counterion dye (Jin and Choi, 2004). However, more experimentation is needed to improve and further characterize this kind of luminescent dye.

CONCLUSION

In this manuscript, we presented the synthesis and characterization of the new *fac*-[Re(CO)$_3$(**deeb**)**B2**]$^+$ complex. We also assessed photophysical properties, suggesting that **B2** may be a weaker electron-donating group than −Br or may exert a withdrawing effect as an ancillary ligand concerning the Re(I) core. Relativistic studies corroborated these experimental results. Moreover, *fac*-[Re(CO)$_3$(**deeb**)**B2**]$^+$ also exhibited good features to be used directly as a fluorophore. Finally, we showed the potential of *fac*-[Re(CO)$_3$(**deeb**)**B2**]$^+$ as a fluorescent protein dye, opening a new window for novel applications of this kind of rhenium(I) tricarbonyl complex.

DATA AVAILABILITY STATEMENT

The original contributions presented in the study are included in the article/**Supplementary Material**; further inquiries can be directed to the corresponding authors.

AUTHOR CONTRIBUTIONS

AC performed design, synthesis, and characterization of the complexes, discussion of all the experiments, theoretical calculations, and paper editing. MG performed electrochemical studies and the associated discussion. ES-C performed relativistic DFT calculations. DP-H performed SOC-TDDFT calculations and discussion of the quantum chemistry section. WS performed photophysical experiments. GM discussed the photophysical experiments. MP discussed the chemical characterization data. IC discussed about the synthesis procedure. AV discussed about the synthesis procedure. JF conceived the study, discussed all the figures and results, made the experiments and figures in the biological section, supervised and directed all the experiments in the biological section, and wrote and edited the manuscript.

FUNDING

This work was funded by FONDECYT de Iniciación 11170637 (ANID) and Núcleo UNAB DI-02-19/N. J. A. Fuentes thanks FONDECYT 1181638 (ANID).

ACKNOWLEDGMENTS

AV thanks Financiamiento Basal AFB 180001 (CEDENNA). MP thanks funding from Dirección de Investigación y Postgrado (FQYF, UC, Chile). Special thanks to María A. del Valle (UC, Chile) and Annie Castel (U. Paul Sabatier, France) for instrumental facilities, and Juan Manuel Manríquez (UC, retired). Dedicated to the Emeritus Professor R. Arratia-Pérez (UNAB, Chile).

SUPPLEMENTARY MATERIAL

The Supplementary Material for this article can be found online at: https://www.frontiersin.org/articles/10.3389/fchem.2021.647816/full#supplementary-material.

REFERENCES

Abdellah, M., El-Zohry, A. M., Antila, L. J., Windle, C. D., Reisner, E., and Hammarström, L. (2017). Time-resolved IR spectroscopy reveals a mechanism with TiO_2 as a reversible electron acceptor in a TiO_2-Re catalyst system for CO_2 photoreduction. *J. Am. Chem. Soc.* 139, 1226–1232. doi:10.1021/jacs.6b11308

Anton, J., Fricke, B., and Engel, E. (2004). Noncollinear and collinear relativistic density-functional program for electric and magnetic properties of molecules. *Phys. Rev. Appl.* 69, 12505-012505. doi:10.1103/physreva.69.012505

Babak, M. V., Le Faouder, P., Trivelli, X., Venkatesan, G., Bezzubov, S. I., Kajjout, M., et al. (2020). Heteroleptic ruthenium(II) complexes with bathophenanthroline and bathophenanthroline disulfonate disodium salt as fluorescent dyes for in-gel protein staining. *Inorg. Chem.* 59, 4527–4535. doi:10.1021/acs.inorgchem.9b03679

Balaji, S., Mohamed Subarkhan, M. K., Ramesh, R., Wang, H., and Semeril, D. (2020). Synthesis and structure of arene Ru(II) N∧O-chelating complexes: in vitro cytotoxicity and cancer cell death mechanism. *Organometallics* 39, 1366–1375. doi:10.1021/acs.organomet.0c00092

Bell, P. J., and Karuso, P. (2003). Epicocconone, a novel fluorescent compound from the fungus epicoccumnigrum. *J. Am. Chem. Soc.* 125, 9304–9305. doi:10.1021/ja035496+

Berggren, K., Chernokalskaya, E., Steinberg, T. H., Kemper, C., Lopez, M. F., Diwu, Z., et al. (2000). Background-free, high sensitivity staining of proteins in one- and two-dimensional sodium dodecyl sulfate-polyacrylamide gels using a luminescent ruthenium complex. *Electrophoresis.* 21, 2509–2521. doi:10.1002/1522-2683(20000701)21:12<2509::AID-ELPS2509>3.0.CO;2-9

Berríos, P., Fuentes, J. A., Salas, D., Carreño, A., Aldea, P., Fernández, F., et al. (2018). Inhibitory effect of biofilm-forming *Lactobacillus kunkeei* strains against virulent *Pseudomonas aeruginosa in vitro* and in honeycomb moth (*Galleria mellonella*) infection model. *Benef. Microbes* 9, 257–268. doi:10.3920/BM2017.0048

Bickelhaupt, F. M., and Baerends, E. J. (2007). Kohn sham density functional theory: predicting and understanding Chemistry. *Rev. Comput. Chem.* 15. Wiley Online LIbrary. 10.1002/9780470125922.ch1.

Bistoni, G., Rampino, S., Scafuri, N., Ciancaleoni, G., Zuccaccia, D., Belpassi, L., et al. (2016). How π back-donation quantitatively controls the CO stretching response in classical and non-classical metal carbonyl complexes. *Chem. Sci.* 7, 1174–1184. doi:10.1039/c5sc02971f

Bond, A. M., Colton, R., and Mcdonald, M. E. (2002). Chemical and electrochemical studies of tricarbonyl derivatives of manganese and rhenium. *Inorg. Chem.* 17, 2842–2847. doi:10.1021/ic50188a032

Canales, J. C., Carreño, A., Oyarzún, D. P., Manríquez, J. M., and Chávez, I. (2017). A preliminary study on electrocatalytic reduction of CO2 using FAC-Rel(CO)3(4,4'-di-methyl-2,2'-bipyridyl)((E)-2-((3-amino-pyridin-4-ylimno)-methyl)-4,6-di-tert-butylphenol))+ complex. *J. Chil. Chem. Soc.* 62, 3765–3771. doi:10.4067/s0717-97072017000403765

Carreño, A., Páez-Hernández, D., Zúñiga, C., Ramírez-Osorio, A., Nevermann, J., Rivera-Zaldívar, M. M., et al. (2019). Prototypical cis-Ruthenium (II) complexes present differential fluorescent staining in walled-cell models (yeasts). *Chem. Pap.* 73, 1629–1637. doi:10.1007/s11696-019-00714-z

Carreño, A., Aros, A. E., Otero, C., Polanco, R., Gacitúa, M., Arratia-Pérez, R., et al. (2017a). Substituted bidentate and ancillary ligands modulate the bioimaging properties of the classical Re(i) tricarbonyl core with yeasts and bacteria. *New J. Chem.* 41, 2140–2147. doi:10.1039/c6nj03792e

Carreño, A., Gacitúa, M., Fuentes, J. A., Páez-Hernández, D., Araneda, C., Chávez, I., et al. (2016a). Theoretical and experimental characterization of a novel pyridine benzimidazole: suitability for fluorescence staining in cells and antimicrobial properties. *New J. Chem.* 40, 2362–2375. doi:10.1039/c5nj02772a

Carreño, A., Gacitúa, M., Fuentes, J. A., Páez-Hernández, D., Peñaloza, J. P., Otero, C., et al. (2016b). Fluorescence probes for prokaryotic and eukaryotic cells using $Re(CO)_{3+}$complexes with an electron withdrawing ancillary ligand. *New J. Chem.* 40, 7687–7700. doi:10.1039/c6nj00905k

Carreño, A., Gacitúa, M., Molins, E., and Arratia-Pérez, R. (2017b). X-ray diffraction and relativistic DFT studies on the molecular biomarker fac-Re(CO)3(4,4′-dimethyl-2,2′-bpy)(E-2-((3-amino-pyridin-4-ylimino)-methyl)-4,6-di-tert-butylphenol)(PF6). *Chem. Pap.* 71, 2011–2022. doi:10.1007/s11696-017-0196-6

Carreño, A., Gacitua, M., Schott, E., Zarate, X., Manriquez, J. M., Preite, M., et al. (2015). Experimental and theoretical studies of the ancillary ligand (E)-2-((3-amino-pyridin-4-ylimino)-methyl)-4,6-di-tert-butylphenol in the rhenium(I) core. *New J. Chem.* 39, 5725–5734. doi:10.1039/c5nj00772k

Carreño, A., Páez-Hernández, D., Zúñiga, C., Ramírez-Osorio, A., Pizarro, N., Vega, A., et al. (2021). Exploring rhenium (I) complexes as potential fluorophores for walled-cells (yeasts and bacteria): photophysics, biocompatibility, and confocal microscopy. *Dyes Pigm.* 184, 108876. doi:10.1016/j.dyepig.2020.108876

Carreño, A., Solis-Céspedes, E., Páez-Hernández, D., and Arratia-Pérez, R. (2017). Exploring the geometrical and optical properties of neutral rhenium (I) tricarbonyl complex of 1,10-phenanthroline-5,6-diol using relativistic methods. *Chem. Phys. Lett.* 685, 354–362. doi:10.1016/j.cplett.2017.07.058

Czerwieniec, R., Kapturkiewicz, A., Lipkowski, J., and Nowacki, J. (2005). Re(I)(tricarbonyl)$^{+}$ complexes with the 2-(2-pyridyl)-N-methyl-benzimidazole, 2-(2-pyridyl)benzoxazole and 2-(2-pyridyl)benzothiazole ligands - syntheses, structures, electrochemical and spectroscopic studies. *Inorg. Chim. Acta* 358, 2701–2710. doi:10.1016/j.ica.2005.03.013

Del Valle, M. A., Gacitúa, M., Díaz, F. R., Armijo, F., and Río, R. d. (2009). Electrosynthesis of polythiophene nanowires via mesoporous silica thin film templates. *Electrochemistry Commun.* 11, 2117–2120. doi:10.1016/j.elecom.2009.09.009

Del Valle, M. A., Gacitua, M., Diaz, F. R., Armijo, F., and Soto, J. P. (2012). Electrosynthesis and characterization of polythiophene nano-wires/platinum nanoparticles composite electrodes. Study of formic acid electro-catalytic oxidation. *Electrochimica. Acta.* 71, 277–282. doi:10.1016/j.electacta.2012.04.001

Fernández-Moreira, V., Thorp-Greenwood, F. L., and Coogan, M. P. (2010). Application of d6 transition metal complexes in fluorescence cell imaging. *Chem. Commun. (Camb)* 46, 186–202. doi:10.1039/b917757d

Fiorini, V., Bergamini, L., Monti, N., Zacchini, S., Plush, S. E., Massi, M., et al. (2018). Luminescent protein staining with Re(I) tetrazolato complexes. *Dalton Trans.* 47, 9400–9410. doi:10.1039/c8dt02052c

Graham, G., Nairn, R. S., and Bates, G. W. (1978). Polyacrylamide gel staining with Fe2+-bathophenanthroline sulfonate. *Anal. Biochem.* 88, 434–441. doi:10.1016/0003-2697(78)90441-4

Hasselmann, G. M., and Meyer, G. J. (1999a). Diffusion-limited interfacial electron transfer with large apparent driving forces. *J. Phys. Chem. B* 103, 7671–7675. doi:10.1021/jp992086s

Hasselmann, G. M., and Meyer, G. J. (1999b). Sensitization of nanocrystalline TiO2by Re(I) polypyridyl compounds*. *Z. für Physikalische Chem.* 212, 39–44. doi:10.1524/zpch.1999.212.part_1.039

Hess, G. D., Fiedler, T., Hampel, F., and Gladysz, J. A. (2017). Octahedral gyroscope-like molecules consisting of rhenium rotators within cage-like dibridgehead diphosphine stators: syntheses, substitution reactions, structures, and dynamic properties. *Inorg. Chem.* 56, 7454–7469. doi:10.1021/acs.inorgchem.7b00909

Hostachy, S., Policar, C., and Delsuc, N. (2017). Re(I) carbonyl complexes: multimodal platforms for inorganic chemical biology. *Coord. Chem. Rev.* 351, 172–188. doi:10.1016/j.ccr.2017.05.004

Jia, J., Fei, H., and Zhou, M. (2012). Luminescent iridium(III) complexes as novel protein staining agents. *Electrophoresis* 33, 1397–1401. doi:10.1002/elps.201100693

Jin, L. T., and Choi, J. K. (2004). Usefulness of visible dyes for the staining of protein or DNA in electrophoresis. *Electrophoresis* 25, 2429–2438. doi:10.1002/elps.200305995

Kang, Y., Ito, A., Sakuda, E., and Kitamura, N. (2017). Characteristic spectroscopic and photophysical properties of tricarbonyl rhenium(I) complexes having multiple arylborane charge transfer units. *Bcsj* 90, 574–585. doi:10.1246/bcsj.20160398

Kia, R., and Safari, F. (2016). Synthesis, spectral and structural characterization and computational studies of rhenium(I)-tricarbonyl nitrito complexes of 2,2′-bipyridine and 2,9-dimethylphenanthroline ligands: π-Accepting character of the diimine ligands. *Inorg. Chim. Acta* 453, 357–368. doi:10.1016/j.ica.2016.08.041

Kim, K., and Jordan, K. D. (1994). Comparison of density functional and MP2 calculations on the water monomer and dimer. *J. Phys. Chem.* 98, 10089–10094. doi:10.1021/j100091a024

Krause, K., and Klopper, W. (2015). Description of spin-orbit coupling in excited states with two-component methods based on approximate coupled-cluster theory. *J. Chem. Phys.* 142, 104109. doi:10.1063/1.4908536

Lennox, J. C., Kurtz, D. A., Huang, T., and Dempsey, J. L. (2017). Excited-state proton-coupled electron transfer: different avenues for promoting proton/electron movement with solar photons. *ACS Energy Lett.* 2, 1246–1256. doi:10.1021/acsenergylett.7b00063

Lenthe, E. V., Baerends, E. J., and Snijders, J. G. (1993). Relativistic regular two-component Hamiltonians. *J. Chem. Phys.* 99, 4597–4610. doi:10.1063/1.466059

Li, R., Ma, Y., Hu, X., Wu, W., Wu, X., Dong, C., et al. (2020). [Ru(phen)2podppz]$^{2+}$ significantly inhibits glioblastoma growth *in vitro* and vivo with fewer side-effects than cisplatin. *Dalton Trans.* 49, 8864–8871. doi:10.1039/d0dt01877e

Lindley, B. M., Van Alten, R. S., Finger, M., Schendzielorz, F., Würtele, C., Miller, A. J. M., et al. (2018). Mechanism of chemical and electrochemical N_2 splitting by a rhenium pincer complex. *J. Am. Chem. Soc.* 140, 7922–7935. doi:10.1021/jacs.8b03755

Llancalahuen, F. M., Fuentes, J. A., Carreño, A., Zúñiga, C., Páez-Hernández, D., Gacitúa, M., et al. (2018). New properties of a bioinspired pyridine benzimidazole compound as a novel differential staining agent for endoplasmic reticulum and Golgi apparatus in fluorescence live cell imaging. *Front. Chem.* 6, 345. doi:10.3389/fchem.2018.00345

Lo, K. K.-W., Lau, J. S.-Y., Fong, V. W.-Y., and Zhu, N. (2004). Electrochemical, photophysical, and anion-binding properties of a luminescent rhenium(I) polypyridine anthraquinone complex with a thiourea receptor. *Organometallics* 23, 1098–1106. doi:10.1021/om034224c

Macleod-Carey, D., Caramori, G. F., Guajardo-Maturana, R., Paez-Hernandez, D., Muñoz-Castro, A., and Arratia-Perez, R. (2018). Advances in bonding and properties of inorganic systems from relativistic calculations in Latin America. *Int. J. Quan. Chem.* 119, 1–14. doi:10.1002/qua.25777

Maizel, J. V. (2000). SDS polyacrylamide gel electrophoresis. *Trends Biochem. Sci.* 25, 590–592. doi:10.1016/s0968-0004(00)01693-5

Malecka, M., Machura, B., Switlicka, A., Kotowicz, S., Szafraniec-Gorol, G., Siwy, M., et al. (2020). Towards better understanding of photophysical properties of rhenium(I) tricarbonyl complexes with terpy-like ligands. *Spectrochim. Acta. A. Mol. Biomol. Spectrosc.* 231, 118124. doi:10.1016/j.saa.2020.118124

Manbeck, G. F., Fujita, E., and Concepcion, J. J. (2016). Proton-coupled electron transfer in a strongly coupled photosystem II-inspired chromophore-imidazole-phenol complex: stepwise oxidation and concerted reduction. *J. Am. Chem. Soc.* 138, 11536–11549. doi:10.1021/jacs.6b03506

Manbeck, G. F., Muckerman, J. T., Szalda, D. J., Himeda, Y., and Fujita, E. (2015). Push or pull? Proton responsive ligand effects in rhenium tricarbonyl CO_2 reduction catalysts. *J. Phys. Chem. B.* 119, 7457–7466. doi:10.1021/jp511131x

Maroń, A. M., Szlapa-Kula, A., Matussek, M., Kruszynski, R., Siwy, M., Janeczek, H., et al. (2020). Photoluminescence enhancement of Re(I) carbonyl complexes bearing D-A and D-π-A ligands. *Dalton Trans.* 49, 4441–4453. doi:10.1039/c9dt04871e

Nastasi, F., Puntoriero, F., Natali, M., Mba, M., Maggini, M., Mussini, P., et al. (2015). Photoinduced intercomponent excited-state decays in a molecular dyad made of a dinuclear rhenium(I) chromophore and a fullerene electron acceptor unit. *Photochem. Photobiol. Sci.* 14, 909–918. doi:10.1039/c4pp00301b

Nevermann, J., Silva, A., Otero, C., Oyarzún, D. P., Barrera, B., Gil, F., et al. (2019). Identification of genes involved in biogenesis of outer membrane vesicles (OMVs) in *Salmonella enterica* serovar Typhi. *Front. Microbiol.* 10, 104. doi:10.3389/fmicb.2019.00104

Nomrowski, J., and Wenger, O. S. (2015). Photoinduced PCET in ruthenium-phenol systems: thermodynamic equivalence of uni- and bidirectional reactions. *Inorg. Chem.* 54, 3680–3687. doi:10.1021/acs.inorgchem.5b00318

Otero, C., Carreño, A., Polanco, R., Llancalahuen, F. M., Arratia-Pérez, R., Gacitúa, M., et al. (2019). Rhenium (I) complexes as probes for prokaryotic and fungal cells by fluorescence microscopy: do ligands matter? *Front. Chem.* 7, 454. doi:10.3389/fchem.2019.00454

Pannwitz, A., and Wenger, O. S. (2019). Recent advances in bioinspired proton-coupled electron transfer. *Dalton Trans.* 48, 5861–5868. doi:10.1039/c8dt04373f

Patton, W. F. (2002). Detection technologies in proteome analysis. *J. Chromatogr. B. Analyt. Technol. Biomed. Life Sci.* 771, 3–31. doi:10.1016/s1570-0232(02)00043-0

Prado, F., Sousa, S., Machado, A. E., and Patrocinio, A. O. (2016). Influence of the protonatable site in the photo-induced proton-coupled electron transfer between rhenium(I) polypyridyl complexes and hydroquinone. *J. Braz. Chem. Soc.* 46, 1517–1526. doi:10.21577/0103-5053.20170022

Rabilloud, T., Strub, J. M., Luche, S., Van Dorsselaer, A., and Lunardi, J. (2001). A comparison between Sypro Ruby and ruthenium II tris (bathophenanthroline disulfonate) as fluorescent stains for protein detection in gels. *Proteomics* 1, 699–704. doi:10.1002/1615-9861(200104)1:5<699::AID-PROT699>3.0.CO;2-C

Rabilloud, T. (1990). Mechanisms of protein silver staining in polyacrylamide gels: a 10-year synthesis. *Electrophoresis* 11, 785–794. doi:10.1002/elps.1150111003

Ramírez, C., Del Valle, M. A., Isaacs, M., and Armijo, F. (2016). Electrochemical oxidation of catecholamines on fluorine-doped SnO_2 substrates. Square-wave voltammetric method for methyldopa determination in pharmaceutical dosage formsSquare-wave voltammetric method for methyldopa determination in pharmaceutical dosage forms. *Electrochimica. Acta.* 199, 227–233. doi:10.1016/j.electacta.2016.03.093

Rojas-Poblete, M., Carreño, A., Gacitúa, M., Páez-Hernández, D., Rabanal-León, W. A., and Arratia-Pérez, R. (2018). Electrochemical behaviors and relativistic DFT calculations to understand the terminal ligand influence on the $[Re6(\mu3\text{-}Q)8X6]^{4-}$ clusters. *New J. Chem.* 42, 5471–5478. doi:10.1039/c7nj05114j

Samdin, T. D., Wierzbicki, M., Kreutzer, A. G., Howitz, W. J., Valenzuela, M., Smith, A., et al. (2020). Effects of N-terminal residues on the assembly of constrained β-hairpin peptides derived from a*β*. *J. Am. Chem. Soc.* 142, 11593–11601. doi:10.1021/jacs.0c05186

Steinberg, T. H., Chernokalskaya, E., Berggren, K., Lopez, M. F., Diwu, Z., Haugland, R. P., et al. (2000). Ultrasensitive fluorescence protein detection in isoelectric focusing gels using a ruthenium metal chelate stain. *Electrophoresis* 21, 486–496. doi:10.1002/(SICI)1522-2683(20000201)21:3<486::AID-ELPS486>3.0.CO;2-Q

Stephens, P. J., Devlin, F. J., Chabalowski, C. F., and Frisch, M. J. (1994). *Ab initio* calculation of vibrational absorption and circular dichroism spectra using density functional force fields. *J. Phys. Chem.* 98, 11623–11627. doi:10.1021/j100096a001

Sundaram, R. K., Balasubramaniyan, N., and Sundaram, P. (2012). Protein stains and applications. *Methods Mol. Biol.* 869, 451–464. doi:10.1007/978-1-61779-821-4_39

Te Velde, G., Bickelhaupt, F. M., Baerends, E. J., Fonseca Guerra, C., Van Gisbergen, S. J. A., Snijders, J. G., et al. (2001). Chemistry with ADF. *J. Comput. Chem.* 22, 931–967. doi:10.1002/jcc.1056

Thorp-Greenwood, F. L., Balasingham, R. G., and Coogan, M. P. (2012). Organometallic complexes of transition metals in luminescent cell imaging applications. *J. Organomet. Chem.* 714, 12–21. doi:10.1016/j.jorganchem.2012.01.020

Thorp-Greenwood, F. L., Pritchard, V. E., Coogan, M. P., and Hardie, M. J. (2016). Tris(rhenium fac-tricarbonyl) polypyridine functionalized cyclotriguaiacylene ligands with rich and varied emission. *Organometallics* 35, 1632–1642. doi:10.1021/acs.organomet.6b00099

Tian, M., Li, J., Zhang, S., Guo, L., He, X., Kong, D., et al. (2017). Half-sandwich ruthenium(II) complexes containing NN-chelated imino-pyridyl ligands that are selectively toxic to cancer cells. *Chem. Commun. (Camb)* 53, 12810–12813. doi:10.1039/c7cc08270c

Van Lenthe, E., and Baerends, E. J. (2003). Optimized Slater-type basis sets for the elements 1-118. *J. Comput. Chem.* 24, 1142–1156. doi:10.1002/jcc.10255

Wallace, L., and Rillema, D. P. (1993). Photophysical properties of rhenium(I) tricarbonyl complexes containing alkyl- and aryl-substituted phenanthrolines as ligands. *Inorg. Chem.* 32, 3836–3843. doi:10.1021/ic00070a012

Wang, F., and Ziegler, T. (2005). A simplified relativistic time-dependent density-functional theory formalism for the calculations of excitation energies including spin-orbit coupling effect. *J. Chem. Phys.* 123, 154102. doi:10.1063/1.2061187

Wirth, P. J., and Romano, A. (1995). Staining methods in gel electrophoresis, including the use of multiple detection methods. *J. Chromatogr. A.* 698, 123–143. doi:10.1016/0021-9673(94)00879-e

Xu, Z., Kong, D., He, X., Guo, L., Ge, X., Liu, X., et al. (2018). Mitochondria-targeted half-sandwich rutheniumII diimine complexes: anticancer and antimetastasis via ROS-mediated signalling. *Inorg. Chem. Front.* 5, 2100–2105. doi:10.1039/c8qi00476e

Zeng, Q., Messaoudani, M., Vlček, A., and Hartl, F. (2012). Electrochemical reductive deprotonation of an imidazole ligand in a bipyridine tricarbonyl rhenium(I) complex. *Eur. J. Inorg. Chem.* 2012, 471–474. doi:10.1002/ejic.201101100

Zewert, T. E., and Harrington, M. G. (1993). Protein electrophoresis. *Curr. Opin. Biotechnol.* 4, 3–8. doi:10.1016/0958-1669(93)90024-q

Zhang, M. T., Irebo, T., Johansson, O., and Hammarström, L. (2011). Proton-coupled electron transfer from tyrosine: a strong rate dependence on intramolecular proton transfer distance. *J. Am. Chem. Soc.* 133, 13224–13227. doi:10.1021/ja203483j

Conflict of Interest: The authors declare that the research was conducted in the absence of any commercial or financial relationships that could be construed as a potential conflict of interest.